C. R. Mecanique 341 (2013) 230–237

Contents lists available at SciVerse ScienceDirect

Comptes Rendus Mecanique

www.sciencedirect.com

Combustion, flow and spray dynamics for aerospace propulsion

Soot prediction by Large-Eddy Simulation of complex geometry combustion chambers

Prédiction des suies par simulation aux grandes échelles de chambres de combustion à géométrie complexe

Guillaume Lecocq *, Ignacio Hernández, Damien Poitou, Eléonore Riber, Bénédicte Cuenot

CERFACS, CFD Team, 42, avenue G. Coriolis, 31057 Toulouse cedex 01, France

ARTICLE INFO

Article history:
Available online 3 January 2013

Keywords:
Combustion
Soot modeling
Complex chemistry
Large-Eddy Simulation

Mots-clés :
Combustion
Modélisation des suies
Chimie complexe
Simulation aux grandes échelles

ABSTRACT

This article is dedicated to the modeling of soot production in Large-Eddy Simulations (LES) of complex geometries. Such computations impose a trade-off between accuracy and CPU cost which limits the choice of soot models to semi-empirical ones. As the presence of acetylene is a necessary condition for soot inception, the Leung et al. model that accounts for this feature is chosen and used in this work. However, acetylene concentration is not provided by the reduced chemistries used in LES of complex geometries and a methodology has been developed to predict this key species through a tabulation technique. With this methodology, the model of Leung et al. is first tested and validated against measured laminar premixed flames. Then, the soot prediction method is applied to the LES of the combustion chamber of a helicopter engine.

RÉSUMÉ

Cet article aborde la modélisation de la production des suies pour des simulations aux grandes échelles (SGE) de géométries complexes. De tels calculs imposent un compromis entre précision et temps de calcul qui limite le choix des modèles de suie aux approches semi-empiriques. La présence d'acétylène étant une condition nécessaire à la nucléation des particules de suie, le modèle de Leung et al. qui intègre cette caractéristique est choisi et utilisé dans ce travail. Cependant, la concentration d'acétylène n'est pas fournie par les chimies réduites utilisées dans les SGE de géométries complexes et une méthodologie a été développée pour prédire cette espèce clé à travers une technique de tabulation. Avec cette méthodologie, le modèle de Leung et al. est tout d'abord testé et validé à partir de mesures de flammes laminaires prémélangées. Ensuite, la méthode de prédiction des suies est appliquée à la SGE de la chambre de combustion d'un moteur d'hélicoptère.

* Corresponding author.
E-mail address: lecocq@cerfacs.fr (G. Lecocq).

1631-0721/$ – see front matter
http://dx.doi.org/10.1016/j.crme.2012.10.002

1. Introduction

Soot prediction remains nowadays both a necessity and a challenge. It is a necessity because soot particles have a non-negligible impact on environment at several scales. They are known to be carcinogen for human beings [1]. They are also suspected to trigger the formation of contrails [2], whose long term presence impacts the local climate. For engineering applications soot matters as well, either positively or negatively. Soot enhances heat fluxes in furnaces [3], corresponding to a positive effect on the industrial process. Their presence in the combustion chamber of an aircraft engine affects the thermal balance and then the gases temperature seen by the turbine blades, whose life expectancy is a key issue for engine manufacturers. The blades can also be physically damaged by soot particle collisions.

Several approaches were used to model soot emitted by combustion of kerosene surrogates. For jet flames, soot was notably modeled by a sectional approach [4], which is among the most complex formalisms and in simpler way, with a semi-empirical model [5].

In the context of Large-Eddy Simulation (LES) of complex geometries, the choice of the soot modeling approach is limited by a trade-off between CPU cost and accuracy. The semi-empirical soot model of Leung et al. [6] is chosen here. It requires the concentration of acetylene to predict soot particle nucleation, a species which is not predicted by the usual reduced chemistries employed in LES [7]. Therefore a methodology is developed, described in the first part, that allows to recover detailed chemistry effects from simplified chemistry. Then, the soot model is tested in the case of laminar rich premixed ethylene/air flames. Finally, the model is applied to the prediction of soot in an industrial configuration: the combustion chamber of a helicopter engine in which kerosene is burned with air at high pressure and temperature.

2. Method for soot modeling in a CFD solver

Soot prediction is a challenge, because soot is the final product of complex processes, whose modeling CPU cost can be very high. Indeed, nucleation, *i.e.* the formation of the first particles, occurs through collision of polycyclic aromatic hydrocarbons (PAHs), whose formation paths have to be understood and modeled. This step is followed by simultaneous phenomena. The soot particle size increases due to mass addition on the surface of the particle: by growth rate (C_2H_2 addition) and condensation (PAHs addition). It can also decrease via oxidation by both O_2 and OH. Finally, soot can aggregate. Accounting for all these physical and chemical features in details is again very demanding in terms of computing resources.

The soot models are varied, as semi-empirical [6,8,9], sectional approaches [10], stochastic models [11] or method of moments [12] can be used. As a first step, and due to CPU cost, semi-empirical models are chosen for the LES of complex geometries. The soot is described through two transport quantities: the local soot mass fraction Y_s and the number density n of soot particles. One of the main differences between semi-empirical models is the description of the inception phase, in particular the choice of the precursor species. Moss et al. [8] choose the fuel as the precursor, Leung et al. [6] base their model on C_2H_2 while Di Domenico et al. [9] use a sectional method to model the PAHs, the collision of the PAHs of the highest class leading to nucleation.

The soot community [13,14] agrees on the necessary presence of C_2H_2 for soot nucleation. Both the models of Leung et al. and Di Domenico et al. present this characteristic, but the first one is preferred, due to its higher simplicity and lower CPU cost (fewer transport equations to solve).

The combustion is often modeled with a simplified chemistry in LES solvers. In order to use the Leung et al. model, a strategy enabling to predict acetylene has to be proposed.

2.1. Prediction of acetylene

When dealing with minor species prediction, tabulation methods, such as FPI [15] come quickly to mind. This latter method consists in computing *a priori* a set of laminar premixed flames accounting for detailed chemistry effects, each flame being characterized by a mixture fraction Z. A FPI table is generated in which all physical quantities φ (chemical species mass fractions, temperature, reaction rates, ...) linked to the flame structure can be read as: $\varphi(Z, c)$ where c is the progress variable, *i.e.* a monotonic variable whose value is 0 in fresh gases and 1 in burned gases. Usually, an equation is solved for c with appropriate closure models. Here a different approach is used, where c is reconstructed from the reduced chemistry calculation.

This approach is investigated, using AVBP [16], a massively parallel code that solves the compressible Navier–Stokes equations together with conservation equations for energy and chemical species on unstructured or hybrid meshes. It is used for the case of a one-dimensional laminar rich premixed kerosene/air flame, under thermodynamic conditions representative of a helicopter engine. The reduced chemistry 2*S_KERO_BFER* [7] (*BFER* in the following) is used. A reference is provided by the same flame (equivalence ratio, fresh gases temperature, pressure) computed with Cantera [17] using a complex chemistry described by the kinetics of Luche (91 chemical species, 991 reactions) [18]. The composition of the kerosene surrogate is the one proposed by Luche [18] and is given in Table 1.

A FPI table has been created from the Cantera solution and stores $\varphi(c)$ where $\varphi = Y_{C_2H_2}, Y_{OH}, T$. 100 points discretize the progress variable space.

Table 1
Composition of the kerosene surrogate.

Species	Mass fraction (%)
n-decane	76.7
n-propylbenzene	13.2
n-propylcyclohexane	10.1

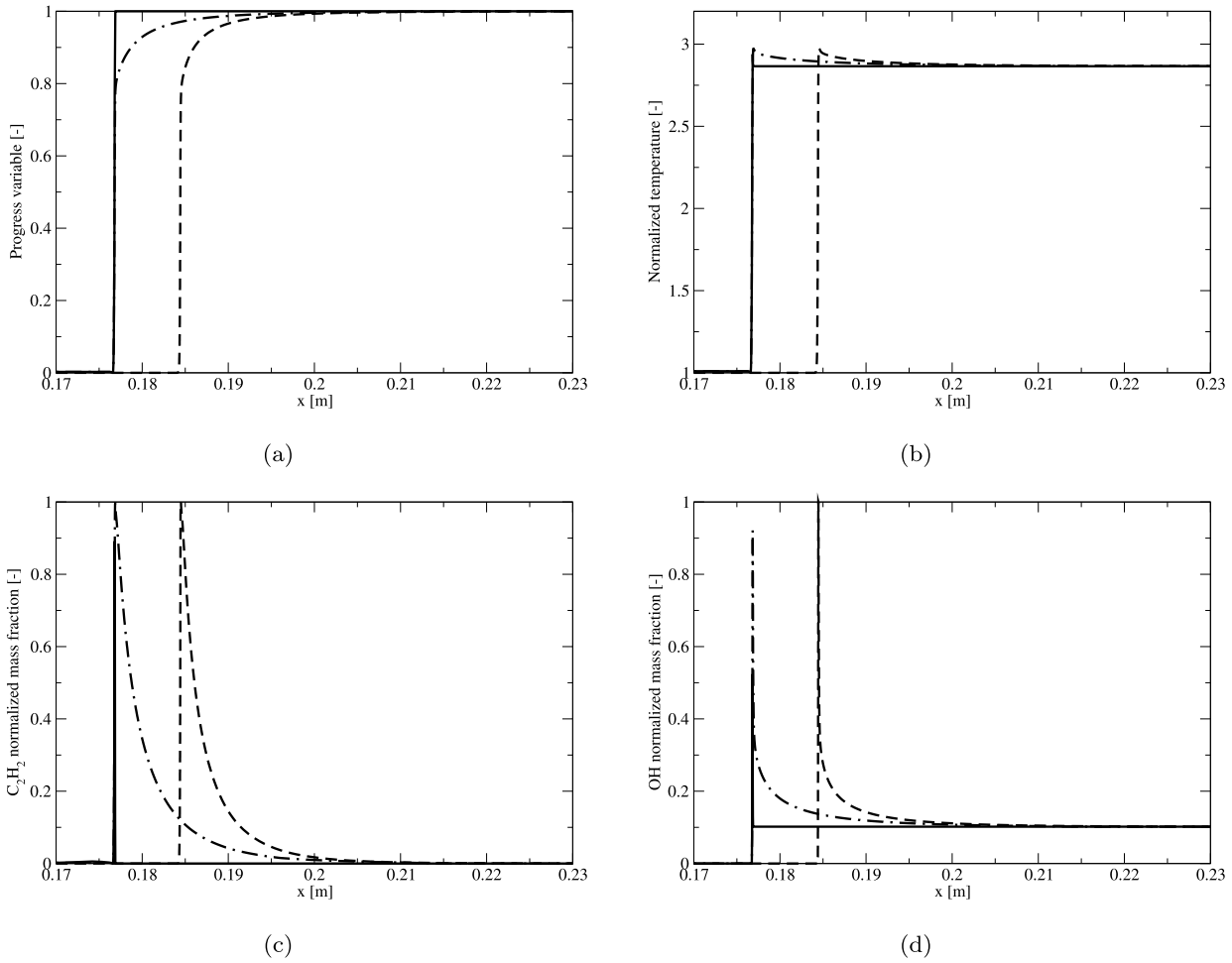

Fig. 1. Profiles of progress variable (a), normalized temperature (b), C_2H_2 (c) and OH (d) mass fractions. Dash line: Cantera computation, line: c^{BFER} (or quantity interpolated on this profile), dot–dash line: c^{bg} (or quantity interpolated on this profile).

2.1.1. Strategy I

Here another definition of the progress variable for 2-step chemistry, c^{BFER} is based on fuel (lean combustion) or oxidizer (rich combustion) consumption. It leads to $c^{BFER} = \max(c^{lean}, c^{rich})$ where:

$$c^{lean} = 1 - \frac{Y_F}{ZY_{F,f}}, \qquad c^{rich} = 1 - \frac{Y_{O_2}}{(1-Z)Y_{O_2,o}} \tag{1}$$

where $Y_{O_2,o}$ is the mass fraction of O_2 in the oxidizer stream and $Y_{F,f}$ is the mass fraction of fuel in the fuel stream. Due to its definition, c^{BFER} captures combustion occurring under a premixed flame mode.

For tabulated chemistry strategies, the progress variable is often defined as [19]: $c^{tab} = (Y_{CO} + Y_{CO_2})/(Y_{CO} + Y_{CO_2})^{eq} = Y_c/Y_c^{eq}$, where the superscript *eq* denotes thermo-chemical equilibrium values.

The progress variables c^{BFER} (obtained with AVBP) and c^{tab} (obtained with Cantera) are compared in Fig. 1 (where the profiles are shifted for clarity). The profiles are similar until a value of about 0.8. While the *BFER* progress variable evolves quickly towards equilibrium, c^{tab} evolves more slowly, due to the existence of a post-flame zone with slow chemical kinetics.

The profiles of $Y_{C_2H_2}(c^{BFER})$, $Y_{OH}(c^{BFER})$ and $T(c^{BFER})$ are then built in AVBP and plotted in Fig. 1(b)–(d), normalized by the maximum value for mass fractions and inlet value for temperature. Whereas the temperature profile is correctly recovered,

neglecting the post-flame region enables to recover a peak of C_2H_2, but not the slow decay on the burned gases side. The consequence for soot will be a significant underestimation, as the absence of C_2H_2 in the post-flame drastically limits both nucleation and surface growth processes.

2.1.2. Strategy II

To improve the description of acetylene, a new progress variable c^{bg} is introduced in AVBP. It is defined, by analogy with the work of Fiorina et al. [19] as: $c^{bg} = Y_c^{bg}/Y_c^{eq}$. The transport equation of Y_c^{bg} reads:

$$\frac{\partial \rho Y_c^{bg}}{\partial t} + \nabla \cdot \left(\rho \mathbf{u} Y_c^{bg}\right) = \nabla \cdot \left(\rho D \nabla Y_c^{bg}\right) + \rho \dot{\omega}_{Y_c}^{bg} \tag{2}$$

The reaction rate appearing in Eq. (2) is built to correct the progress variable profile used to interpolate in the FPI table, following:

- if $c^{BFER} < c^*$ then $\dot{\omega}_{Y_c}^{bg} = \dot{\omega}_c^{BFER} Y_c^{eq}$,
- else $\dot{\omega}_{Y_c}^{bg} = \dot{\omega}_{Y_c}^{tab}(c^{bg})$.

The value of c^* indicates the value of c^{BFER} from which the post-flame is modeled through tabulated chemistry. The choice of c^* is constrained as follows:

- it should be greater than zero, otherwise the post-flame zone would not be anchored to the flame front located by c^{BFER};
- because the post-flame zone (visible on the c^{tab} profile) exists for values of c^{BFER} roughly higher than 0.8, c^* should be lower than this value.

Finally c^* is set to 0.5.

For coding reasons, the quantity $\dot{\omega}_c^{BFER}$ is written in the solver as: $(c^{BFER} - c^{bg})/\tau^*$, τ^* being of the order of few time steps. Such relaxation formulation has been used previously for implementing chemical species reaction rates [20].

Fig. 1 highlights that the profile obtained for c^{bg} has the same shape as the profile of the complex chemistry progress variable. The profiles $Y_{C_2H_2}(c^{bg})$, $Y_{OH}(c^{bg})$ and $T(c^{bg})$, reconstructed in AVBP and represented in Fig. 1 show a very good agreement with the structure of the flame computed with Cantera. Strategy II is retained and will supply the mass fractions of O_2, OH, C_2H_2 and the temperature for the soot model.

2.2. The Leung et al. semi-empirical soot model

The set of transport equations writes, in laminar regime, for the Leung et al. model:

$$\frac{\partial \rho n}{\partial t} + \nabla \cdot (\rho \mathbf{u} n) = k_T \nabla \cdot \left(\rho \nu n \frac{\nabla T}{T}\right) + \frac{2}{C_{min}} N_A k_1(T)[C_2H_2] - 2C_a \left(\frac{6M_s}{\pi \rho_s}\right)^{1/6} \left(\frac{6\kappa T}{\rho_s}\right)^{1/2} (\rho n)^{11/6} \left(\frac{\rho Y_s}{\rho_s}\right) \tag{3}$$

$$\frac{\partial \rho Y_s}{\partial t} + \nabla \cdot (\rho \mathbf{u} Y_s) = k_T \nabla \cdot \left(\rho \nu Y_s \frac{\nabla T}{T}\right) + k_1(T)[C_2H_2]M_s + k_2(T) M_{C_2H_2} f(S) M_s - \left(k_3(T)[O_2] + k_4(T) X_{OH}\right) S M_s \tag{4}$$

with concentrations in $\mathrm{kmol\,m^{-3}}$.

The first term appearing on the right-hand side (RHS) of Eqs. (3) and (4) models the thermophoretic transport, where the constant k_T is set to 0.54. The second RHS term in both equations accounts for soot particles nucleation. Soot growth rate is modeled by the third RHS term in Eq. (4). It involves a function $f(S)$ where S is the total soot volume surface per volume unit of gas. It is locally known as: $S = (\rho n)\pi d_p^2$, with the mean soot particle diameter d_p. The soot model being linked to monodisperse assumption, this diameter is simply expressed as:

$$d_p = \frac{6}{\pi}\left(\frac{1}{\rho_s}\frac{Y_s}{n}\right)^{1/3} \tag{5}$$

The function was basically proposed to integrate aging effects that lead to a decay of soot surface reactivity. As proposed by Leung et al., here $f(S) = S^{1/2}$.

Oxidation is accounted for with the last term of Eq. (4). The contribution due to the OH radical was added to the original model, the corresponding constants coming from the work of Guo et al. [21]. The last term in Eq. (3) models coagulation, *i.e.* the formation of a bigger spherical soot particle.

Table 2
Constants of the modified Leung et al. model. The functions of temperature $k_i(T)$ of Eqs. (3) and (4) are written as: $k_i(T) = A_i T^{n_i} e^{-T_i/T}$ [s^{-1}].

A_1	A_2	A_3	A_4
0.1×10^5	0.1×10^4	0.1×10^5	106.0
n_1	n_2	n_3	n_4
0	0	0.5	$-1/2$
T_1	T_2	T_3	T_4
21 100	12 100	19 680	0
C_a	ρ_s [kg/m^3]	M_s [kg/kmol]	κ [J/K]
9.0	2000	12.011	1.38×10^{-23}
N_A [particles/kmol]			
6.022×10^{26}			

2.3. Computation of premixed C_2H_4 sooting flames

The combustion in the complex set-up considered mainly occurs under a premixed flame mode. Then, this model is tested against the well-known experimental measurements of Xu et al. [13], carried out for three rich burner-stabilized premixed flames.

2.3.1. Numerical procedure

The structure of the three C_2H_4/air flames is first computed with the Cantera [17] code. Detailed chemistry effects are accounted for, using the UDEL chemical mechanism (70 species, 911 chemical reactions) [22]. In burner-stabilized flames, the thermal phenomenology is complex. Heat losses occur through conduction between the cooled burner and the flame, burned gases radiation and conduction between burned gases and a cool stabilization plate. In order to simply account for all these effects in Cantera, the experimental temperature profile is prescribed, a technique commonly adopted for burner-stabilized flames computations.

The flame solution obtained with Cantera is then used as an input for a home-made post-processing tool *can2soot* [23], which solves the set of equations for Y_s and n. In this procedure, there is no feedback of soot concentration on the gaseous phase.

can2soot uses a first-order finite differences spatial discretization, and the steady-state solution is obtained integrating the equivalent pseudo-transient problem with a first-order (Euler's method) temporal scheme until convergence is reached.

The constants from Leung et al. are kept, apart from the pre-exponential factor linked to the soot surface growth rate whose original value is divided by 6 to match experimental results. The whole parameterization is supplied in Table 2.

Recently, computations of counter-flow diffusion flames have been successfully performed with this method and an additional coupling with a radiative code but an other calibration of the modified Leung et al. model [24].

2.3.2. Results

Fig. 2(a) shows the predicted levels of C_2H_2, compared with the experiment. Correct levels for the three cases are obtained, with a more pronounced difference for the intermediate case. Also the increasing slope seems too fast. Nevertheless, these results allow to consider that neglecting the feedback of soot production on the flame chemistry gives satisfying results. Note also that richer flames produce more C_2H_2, which will promote both nucleation and surface growth.

This is confirmed in Fig. 2(b) where more soot is found for richer flames. The agreement between the predicted levels and the experiments is globally correct. However, far from the burner, the experimental soot profiles tend to level off, while the predicted soot profiles continue to increase. This is explained [13] by HACA theory: the decay of H atoms concentration, induced by the temperature drop, prevents the soot surface activation for growth by C_2H_2 addition. This physical feature is not integrated in the present model, but consequences on the final result should be *a priori* limited as the premixed flame considered in the complex set-up remains short.

To the authors' knowledge, no soot profiles have been measured for kerosene or *n*-decane premixed flames. It is assumed that the behavior of the calibrated soot model, validated against C_2H_4 flames, is generic, soot production being mainly controlled by C_2H_2, O_2, OH and the temperature reached during combustion.

3. Application to the case of a helicopter combustion chamber

3.1. Modeling soot in an LES framework

The LES of the combustion chamber is performed with the AVBP code, evocated in Section 2.1.

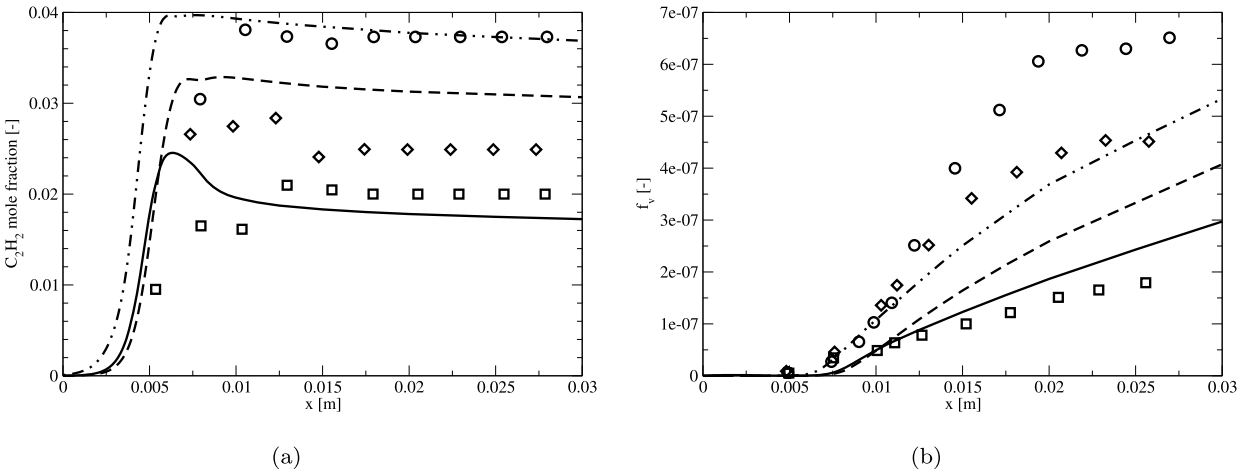

Fig. 2. (a) C_2H_2 mole fraction profiles. (b) Soot volume fractions. Symbols: experiment (squares: $\phi = 2.34$, diamonds: $\phi = 2.64$, circles: $\phi = 2.94$). Lines: computations (solid: $\phi = 2.34$, dash: $\phi = 2.64$, dot–dash: $\phi = 2.94$).

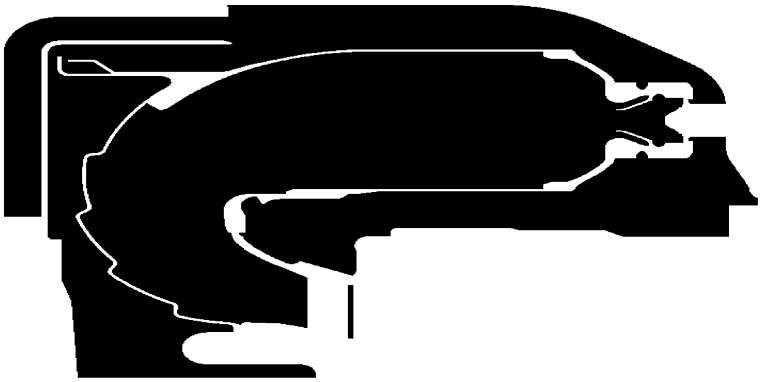

Fig. 3. Cut plane of the computational domain for soot prediction in a sector of an annular combustion chamber of a helicopter engine.

For soot modeling, Eqs. (2), (3) and (4) are filtered, making a non-resolved transport term appear in all equations. This contribution is closed following a classical gradient transport: $\nabla \cdot (\overline{\mathbf{u}\tilde{n}} - \tilde{\mathbf{u}}\tilde{n}) = -\nabla \cdot (D_t \nabla \tilde{n})$ and $\nabla \cdot (\overline{\rho \mathbf{u} \varphi} - \tilde{\rho}\tilde{\mathbf{u}}\tilde{\varphi}) = -\nabla \cdot (\rho D_t \nabla \tilde{\varphi})$ for $\varphi = Y_s$ or $\varphi = Y_c^{bg}$. $D_t = \nu_t / Sc_t$, where ν_t is the turbulent viscosity, Sc_t is the turbulent Schmidt number, equal to 0.6. The filtered source terms in the transport equations of $\tilde{Y}_s$ and $\tilde{n}$ are only functions of the resolved contributions. Sub-grid scale effects on soot production are not accounted for, as such effects have not been quantified yet.

3.2. Set-up

The chosen application is a sector of a helicopter combustion chamber of Turbomeca, which was studied recently by Staffelbach et al. [25,26]. The computational domain is given in Fig. 3 and the operating point considered corresponds to full thrust.

Concerning the mesh, the zone of flame stabilization is refined, leading in total to a discretization of the domain through $11.9 \cdot 10^6$ tetrahedra. Wall laws model the walls behavior and the Lax–Wendroff numerical scheme is used.

Turbulent combustion is addressed through the thickened flame model [27] and the *BFER* chemical mechanism. The sub-grid scale turbulent viscosity is closed with the Smagorinsky model [28].

A FPI table is generated for this application, discretized over 100 points in progress variable space and 100 in mixture fraction space, as the equivalence ratio is non-uniform in the combustion chamber.

The mixture fraction $\tilde{Z}$ is based on carbon atoms. This procedure is rigorous because no differential diffusion effects are accounted for in the chemical transport equations.

It must be pointed out that the mesh, initial solution and numerical set-up have been recovered from a previous work [29]. Strategy II, that allows to build the detailed chemical structure of the flame from a reduced chemistry calculation, appears as a very practical solution to quickly predict pollutants from a computation already performed with reduced chemistry.

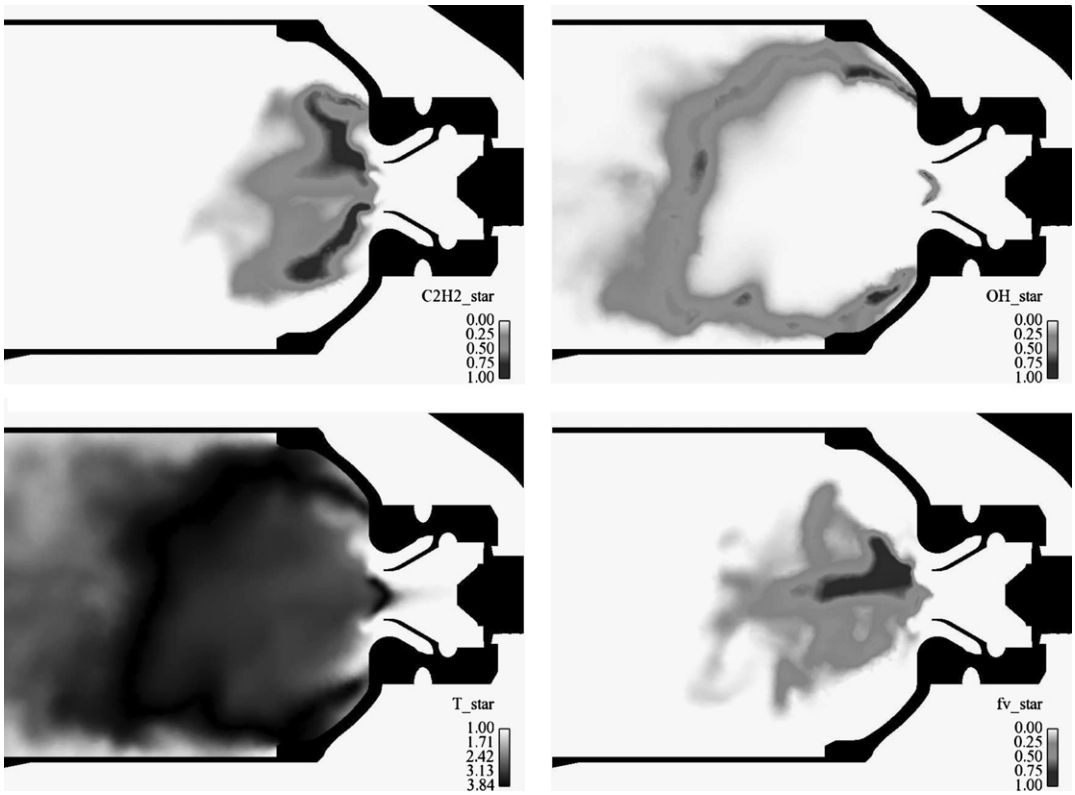

Fig. 4. Instantaneous fields in the vertical cut plane of the burner configuration. Normalized mass fraction of C_2H_2 (top left), OH (top right), temperature (bottom left) and soot volume fraction (bottom right).

3.3. Results

In the helicopter chamber, the combustion is staged: the kerosene/air mixture is first partially burned in the premixed flame zone. Then a secondary combustion occurs in a diffusion flame mode between the burned gases and the fresh dilution air.

The profiles read in the FPI table for an instantaneous solution are shown in Fig. 4. In this representation, fields are normalized as done in Section 2.1.1. C_2H_2 exists only in the rich swirling premixed flame. The maximum quantities of OH are encountered in the highest temperature zone, in which the gases coming from the premixed flame are burned with the dilution air. Having a look at the normalized soot volume fraction field, it can be seen that soot remains confined between the swirling flame and the hot temperature region. It is easily explained, keeping in mind that soot is produced and grows in regions rich in C_2H_2 and is oxidized by O_2 and OH.

A limit of our approach can be underlined here. Indeed, the progress variable is built for premixed flames. Thus, its value remains 1 in the secondary combustion zone, meaning the composition predicted there corresponds to thermo-chemical equilibrium. This is however not true, as non-premixed combustion occurs there. This may have important consequences for soot modeling because at equilibrium, C_2H_2 concentration is zero. Future work is needed to extend the model to non-premixed combustion, using steady or unsteady diffusion flames tables.

4. Conclusions

In this article, a methodology for predicting soot by LES of complex geometries has been proposed. It relies on two ingredients:

(i) the prediction of the key quantities for soot prediction, namely $Y_{C_2H_2}$, Y_{OH}, Y_{O_2}, through a hybrid strategy combining reduced chemistry and FPI tabulation;
(ii) the use of a simple soot model (Leung et al.), widely used in the literature.

The soot model has been tested on a laboratory experiment and provided satisfying results. A strategy has been proposed to account for detailed chemistry effects in an LES computation using reduced chemistry, and proved its potential when compared with a reference Cantera computation.

The modular aspect of the global model is interesting because it allows further improvements. For example, other soot models including PAHs could be theoretically used, the PAHs mass fractions being stored in the chemical table built with prior computations.

Finally, the global method has been applied to the prediction of soot in an industrial combustion chamber. Its practical interest was proved, as a previous computation was re-used for this study. The present work could be nevertheless completed. First, tabulation of flamelets could be considered for modeling minor species mass fractions in the secondary combustion zone. Second, a coupled computation including both the LES and a radiative computation could be carried out. The impact of heat losses should then be added in the chemical tables.

Acknowledgements

The authors wish to thank Dr. Arnaud Trouvé for his advices concerning soot modeling. They also acknowledge Dr. Laurent Gicquel and Elena Collado for providing mesh, initial solution and numerical parameters for the LES. This work was partially funded by the STAE foundation through the ITAAC project and FNRAE within the STRASS project. Furthermore, this work was granted access to the HPC resources of CINES under the allocation 2010-025031 made by GENCI (Grand Equipement National de Calcul Intensif).

References

[1] H. Jung, B. Guo, C. Anastasio, I.M. Kennedy, Quantitative measurements of the generation of hydroxyl radicals by soot particles in a surrogate lung fluid, Atmos. Environ. 40 (6) (2006) 1043–1052.
[2] B. Kärcher, O. Möhler, P.J. DeMott, S. Pechtl, F. Yu, Insights into the role of soot aerosols in cirrus clouds formation, Atmos. Chem. Phys. 7 (2007) 4203–4227.
[3] R. Viskanta, M.P. Mengük, Radiation heat transfer in combustion systems, Prog. Energy Combust. Sci. 13 (1987) 97–160.
[4] M. Saffaripour, P. Zabeti, S.B. Dworkin, Q. Zhang, H. Guo, F. Liu, G.J. Smallwood, M.J. Thomson, A numerical and experimental study of a laminar sooting coflow Jet-A1 diffusion flame, Proc. Combust. Inst. 33 (2011) 601–608.
[5] J.B. Moss, I.M. Askit, Modelling soot formation in a laminar diffusion flame burning a surrogate kerosene fuel, Proc. Combust. Inst. 31 (2007) 3139–3146.
[6] K.M. Leung, R.P. Lindstedt, A simplified reaction mechanism for soot formation in nonpremixed flames, Combust. Flame 87 (1991) 289–305.
[7] B. Franzelli, E. Riber, M. Sanjosé, T. Poinsot, A two-step chemical scheme for Large-Eddy Simulation of kerosene–air flames, Combust. Flame 157 (7) (2010) 1364–1373.
[8] J.B. Moss, C.D. Stewart, K.J. Young, Modeling soot formation and burnout in a high temperature laminar diffusion flame burning under oxygen-enriched conditions, Combust. Flame 101 (1995) 491–500.
[9] M. Di Domenico, P. Gerlinger, M. Aigner, Development and validation of a new soot formation model for gas turbine combustor simulations, Combust. Flame 157 (2010) 246–258.
[10] K. Netzell, H. Lehtiniemi, F. Mauss, Calculating the soot particle size distribution function in turbulent diffusion flames using a sectional method, Proc. Combust. Inst. 31 (1) (2007) 667–674.
[11] J. Singh, Detailed soot modelling in laminar premixed flames, PhD thesis, Cambridge University, July 2006.
[12] M.E. Mueller, G. Blanquart, H. Pitsch, Hybrid method of moments for modeling soot formation and growth, Combust. Flame 156 (6) (June 2009) 1143–1155.
[13] F. Xu, P.B. Sunderland, G.M. Faeth, Soot formation in laminar premixed ethylene/air flames at atmospheric pressure, Combust. Flame 108 (1997) 471–493.
[14] P. Markatou, H. Wang, M. Frenklach, A computational study of sooting limits in laminar premixed flames of ethane, ethylene, and acetylene, Combust. Flame 93 (1993) 467–482.
[15] O. Gicquel, N. Darabiha, D. Thévenin, Laminar premixed hydrogen/air counterflow flame simulations using flame prolongation of ILDM with differential diffusion, Proc. Combust. Inst. 28 (2000) 1901–1908.
[16] V. Moureau, G. Lartigue, Y. Sommerer, C. Angelberger, O. Colin, T. Poinsot, Numerical methods for unsteady compressible multi-component reacting flows on fixed and moving grids, J. Comput. Phys. 202 (2) (2005) 710–736.
[17] David G. Goodwin, Cantera code site, July 2009.
[18] J. Luche, Elaboration of reduced kinetic models of combustion. Application to a kerosene mechanism, PhD thesis, Université d'Orléans, 2003.
[19] B. Fiorina, O. Gicquel, L. Vervisch, S. Carpentier, N. Darabiha, Premixed turbulent combustion modeling using a tabulated detailed chemistry and PDF, Proc. Combust. Inst. 30 (1) (2005) 867–874.
[20] J. Galpin, A. Naudin, L. Vervisch, C. Angelberger, O. Colin, P. Domingo, Large-eddy simulation of a fuel-lean premixed turbulent swirl-burner, Combust. Flame 155 (1–2) (2008) 247–266.
[21] H. Guo, F. Liu, G.J. Smallwood, Soot and NO formation in counterflow ethylene/oxygen/nitrogen diffusion flames, Combust. Theory Model. 8 (3) (2004) 475–489.
[22] S.G. Davis, C.K. Law, H. Wang, Propene pyrolysis and oxidation kinetics in a flow reactor and laminar flames, Combust. Flame 119 (1999) 375–399.
[23] I. Hernández, Modélisation des suies et simulations aux grandes échelles des instabilités thermo-acoustiques, PhD thesis, Université de Toulouse, 2011.
[24] I. Hernandez, G. Lecocq, D. Poitou, E. Riber, B. Cuenot, Computations of soot formation in ethylene/air counterflow diffusion flames and its interaction with radiation, in: INCA Conference, 2011.
[25] G. Staffelbach, L.Y.M. Gicquel, G. Boudier, T. Poinsot, Large eddy simulation of self-excited azimuthal modes in annular combustors, Proc. Combust. Inst. 32 (2009) 2909–2916.
[26] G. Staffelbach, P. Wolf, R. Balakrishnan, A. Roux, T. Poinsot, Azimuthal instabilities in annular combustion chambers, in: Proceedings of the Summer Program, CTR, 2010, pp. 259–269.
[27] O. Colin, F. Ducros, D. Veynante, T. Poinsot, A thickened flame model for large eddy simulations of turbulent premixed combustion, Phys. Fluids 12 (7) (2000) 1843–1863.
[28] J. Smagorinsky, General circulation experiments with the primitive equations: 1. The basic experiment, Mon. Weather Rev. 91 (1963) 99–164.
[29] J. Amaya, E. Collado, B. Cuenot, T. Poinsot, Coupling LES, radiation and structure in gas turbine simulations, in: Proceedings of the Summer Program, CTR, 2010, pp. 239–249.